

An Instrumental Variables Framework to Unite Spatial Confounding Methods

Sophie M. Woodward¹, Mauricio Tec^{1,2}, and Francesca Dominici¹

¹Biostatistics, Harvard University

²Computer Science, Harvard University

November 2024

Abstract

Studies investigating the causal effects of spatially varying exposures on health—such as air pollution, green space, or crime—often rely on observational and spatially indexed data. A prevalent challenge is unmeasured spatial confounding, where an unobserved spatially varying variable affects both exposure and outcome, leading to biased causal estimates and invalid confidence intervals. In this paper, we introduce a general framework based on instrumental variables (IV) that encompasses and unites most of the existing methods designed to account for an unmeasured spatial confounder. We show that a common feature of all existing methods is their reliance on small-scale variation in exposure, which functions as an IV. In this framework, we outline the underlying assumptions and the estimation strategy of each method. Furthermore, we demonstrate that the IV can be used to identify and estimate the exposure-response curve under more relaxed assumptions. We conclude by estimating the exposure-response curve between long-term exposure to fine particulate matter and all-cause mortality among 33,454 zip codes in the United States while adjusting for unmeasured spatial confounding.

Key words: statistics; spatial confounding; instrumental variables; causal inference.

1 Introduction

Studies investigating the effects of environmental exposures on human health often rely on observational, spatially indexed data. For example, one may be interested in examining the effects of exposure to air pollution on hospitalization or lead contamination on child neurological development. Methods of causal inference are crucial to inform decision making in environmental science and epidemiology (Reich et al., 2021; Pearce et al., 2019; Rothman and Greenland, 2005).

A challenge encountered in causal inference studies that rely on observational spatial data is unmeasured spatial confounding. We denote by U an unmeasured confounder that exhibits spatial autocorrelation, that is, two observations in close spatial proximity are highly correlated and their correlation decays as the distance between them grows. Failing to adjust for U results in biased estimates of causal effects and invalid confidence intervals (Robins et al., 2000; Fewell et al., 2007; VanderWeele and Arah, 2011). However, an important aspect of an unmeasured confounder with spatial autocorrelation is that spatial information can be used to adjust for confounding bias, provided that the confounder varies smoothly with space (Gilbert et al., 2021; Tec et al., 2024).

The literature on spatial confounding emphasizes the importance of spatial scale of both the unmeasured confounder and the exposure of interest. Paciorek (2010) examined the bias of the estimated exposure coefficient from both spatial random effects and penalized spline models, assuming a linear model in which Gaussian processes with Matérn correlation generate both the confounder and the exposure. The author found that bias can be reduced only if the unmeasured spatial confounder varies more smoothly across space than the exposure, with smoothness defined by the spatial range parameter of the Matérn correlation. Although recently Khan and Berrett (2023) showed that these findings are sensitive to distributional assumptions, this result has inspired a line of work on spatial confounding that recommends exploiting small-scale or non-spatial variation in exposure to ultimately estimate the statistical parameter of interest (Nobre et al., 2021; Hanks et al., 2015; Dupont et al., 2023; Keller and Szpiro, 2020; Bobb et al., 2022; Guan et al., 2022; Dupont et al., 2022; Giffin et al., 2021; Urdangarin et al., 2024; Thaden and Kneib, 2018; Wiecha and Reich, 2024).

This article shows that six of these methods can be unified under an instrumental variables (IV) framework, in which non-spatial or small-scale variation in the exposure corresponds to the instrument. An IV possesses three key features: 1) *relevance*, meaning the IV influences exposure; 2) *exogeneity*, meaning the IV is independent of unmeasured confounders conditional on covariates; 3) *exclusion restriction*, meaning the IV only affects the outcome through the exposure. IV methods have been a fundamental component of econometrics since the early twentieth century (Wright, 1928; Amemiya, 1974) and have more recently become critical tools in the statistical literature on causal inference (Angrist and Imbens, 1995; Angrist et al., 1996; Imbens, 2014; Baiocchi et al., 2014). While prior work by Giffin et al. (2021) has proposed using instrumental variables to address spatial confounding and interference, the broader link between spatial confounding methods and instrumental variables literature has not yet been fully established. In this paper, we argue that many existing spatial confounding methods *are*, in fact, instrumental variables methods. By drawing this connection, we resolve existing confusion about spatial confounding, revealing a common core principle while distinguishing the unique assumptions underlying each method. We also demonstrate that under our proposed IV framework, we can identify and estimate a causal exposure response curve under less restrictive assumptions than existing methods.

The remainder of this paper is organized as follows. Section 2 introduces a general framework for adjusting for unmeasured spatial confounding using an IV. This framework includes six of the existing methods as special cases. In Section 3, we extend the IV approach by Imbens and Newey (2009) to identify and estimate the exposure-response curve in the context of unmeasured spatial confounding. Section 4 illustrates the performance of the proposed approach in simulation. In Section 5, we estimate the exposure-response curve between long-term average exposure to PM_{2.5} and the all-cause mortality rate in 2014-2016 among Medicare beneficiaries in 33,454 zip codes in the United States while adjusting for unmeasured spatial confounding. Section 6 addresses limitations and presents future directions.

2 Unifying Linear Methods for Spatial Confounding Under an IV Framework

In this section, we present a framework for adjusting for unmeasured spatial confounding using an IV. This framework encompasses six existing spatial confounding methods as special cases and further clarifies the distinct underlying assumptions and estimation strategy that each method employs (Dupont et al., 2022; Urdangarin et al., 2024; Keller and Szpiro, 2020; Guan et al., 2022; Thaden and Kneib, 2018; Wiecha and Reich, 2024).

We introduce the following notation. Let $\mathbf{A} = (A_1, \dots, A_n)^T$, $\mathbf{Y} = (Y_1, \dots, Y_n)^T$, $\mathbf{U} = (U_1, \dots, U_n)^T$, denote exposure, response, and unmeasured confounder, respectively, measured for n units with corresponding spatial coordinates S_1, \dots, S_n . We keep notation general, so that we can accommodate both geostatistical data (randomly sampled S_i) and areal data (fixed S_i , such as the centroids of areal units). For now, we omit measured confounders for simplicity.

We first illustrate the framework in the context of the unsmoothed spatial+ method (Dupont et al., 2022). Analyzing this specific case will help build intuition for the broader framework by clarifying key components. We subsequently formalize our framework and briefly classify the remaining methods within it.

2.1 Spatial+ as an IV method

We begin by reviewing the fundamentals of the spatial+ method (Dupont et al., 2022). The data generation process assumes that

$$\begin{aligned} A_i &= g(S_i) + \epsilon_i^A, \\ Y_i &= \beta_0 + \beta A_i + f(S_i) + \epsilon_i^Y \end{aligned}$$

where f, g are unknown, fixed, bounded functions. This scenario exemplifies unmeasured spatial confounding, because the unobserved function $f(S)$ represents an unmeasured spatial confounder: it directly influences the outcome, correlates with exposure through g , and exhibits spatial autocorrelation. Defining $\epsilon_i = f(S_i) + \epsilon_i^Y$, we observe that an ordinary least squares regression of Y on A , without accounting for S , will result in a biased estimate of β due to the correlation between exposure A and ϵ . Spatial+ mitigates this spatial confounding bias via a two-stage procedure.

1. Regress exposure A on a smooth function of spatial coordinates S (typically a thin plate spline) to obtain the fitted values \hat{g} and residuals $A - \hat{g}(S) = \hat{\epsilon}^A$.
2. Regress outcome Y on first-stage residuals $A - \hat{g}(S) = \hat{\epsilon}^A$ and a thin plate spline of spatial coordinates S . The dimension of the thin plate spline basis used in this stage is identical to that of stage 1. The estimated coefficient of $\hat{\epsilon}^A$ yields the final estimate of the statistical parameter β .

Here is the crucial observation: the validity of this method relies on the assumption that the estimated residual $\hat{\epsilon}^A$ of the first stage regression is not correlated with the unobserved spatial function $f(S)$, which represents the unmeasured confounder. To see this, observe that the resulting estimate of β from stage 2 converges in probability to

$$\frac{\text{Cov}(Y, \hat{\epsilon}^A)}{\text{Var}(\hat{\epsilon}^A)} = \frac{\text{Cov}(\beta_0 + \beta A + \epsilon, \hat{\epsilon}^A)}{\text{Var}(\hat{\epsilon}^A)} = \beta + \frac{\text{Cov}(\epsilon, \hat{\epsilon}^A)}{\text{Var}(\hat{\epsilon}^A)} = \beta,$$

where the last equality holds if and only if $\hat{\epsilon}^A$ is uncorrelated with ϵ , or equivalently, if $\hat{\epsilon}^A$ is uncorrelated with $f(S)$. It is also required that $\text{Var}(\hat{\epsilon}^A) \neq 0$, i.e., exposure A cannot be collinear with the spatial basis.

This observation demonstrates that spatial+ can be viewed as an instrumental variables method, in which $A - \hat{g}(S) = \hat{\epsilon}^A$ corresponds to the instrument. First, $\hat{\epsilon}^A$ is *relevant*, since $\text{Cov}(A, \hat{\epsilon}^A) = \text{Cov}(\hat{\epsilon}^A + \hat{g}(S), \hat{\epsilon}^A) = \text{Var}(\hat{\epsilon}^A)$. Second, it is assumed that $\hat{\epsilon}^A$ is *exogenous*, since the validity of unsmoothed spatial+ relies on $\text{Cor}(\hat{\epsilon}^A, \epsilon) = \text{Cor}(\hat{\epsilon}^A, f(S)) = 0$. Third, $\hat{\epsilon}^A$ obeys *exclusion-restriction*, which is implicit in the functional form of the data-generating process. In fact, unsmoothed spatial+ is equivalent to two-stage least squares—which is a technique commonly used in IV settings—since

an identical estimate of β could be obtained simply by regressing Y on the instrument $\hat{\epsilon}^A$ in the second stage.

There are several takeaways here that motivate a general framework uniting spatial confounding methods under a common set of assumptions. Unsmoothed spatial+ relies on the assumption that exposure can be additively decomposed into two random variables, $\hat{g}(S)$ and $A - \hat{g}(S)$, such that $\hat{g}(S)$ is correlated with the unmeasured confounder and $A - \hat{g}(S)$ is uncorrelated with the unmeasured confounder. Furthermore, $A - \hat{g}(S)$, which can be viewed as an instrument, must have non-zero variance to ensure the identifiability of β . In the context of spatial+, this means that exposure must exhibit variation that is not spanned by the spatial basis that is used in the thin-plate spline regressions.

2.2 IV Framework that Unites Spatial Confounding Methods

We now present our framework unifying six prominent spatial confounding methods under the IV umbrella. All methods share four fundamental assumptions based on implicitly decomposing the treatment in terms of confounded and unconfounded components—as with the case of spatial+. As shown in Table 1, the explicit values of these components, A_C and A_{UC} , is what differentiates each method. The assumptions are:

Assumption 1 (Linear outcome model). $Y_i = \beta_0 + \beta A_i + \epsilon_i$

Assumption 2 (Additive decomposition of exposure). $A_i = A_{C_i} + A_{UC_i}$

Assumption 3 (A_{UC} uncorrelated with A_C). $A_{C_i} \perp A_{UC_i}$

Assumption 4 (A_{UC} uncorrelated with error). $\epsilon_i \perp A_{UC_i}$

where \perp denotes orthogonality (zero correlation). Here, A_C and A_{UC} are two random variables whose sum equals the exposure A . A_C and A_{UC} are correlated and uncorrelated, respectively, with the spatial error ϵ . (In spatial+, we had $A_C = \hat{g}(S)$ and $A_{UC} = \hat{\epsilon}^A$.) Although typically omitted from the data-generating model, the unmeasured confounder may be encoded in the error ϵ , for example $\epsilon_i = U_i + \epsilon_i^Y$ where ϵ_i^Y is i.i.d. exogenous error.

We argue that A_{UC} is an instrumental variable in the following way. First, A_{UC} is *relevant*: this is encoded in Assumptions 2 and 3, which implies that $\text{Cov}(A, A_{UC}) = \text{Cov}(A_C + A_{UC}, A_{UC}) = \text{Var}(A_{UC})$. Therefore, as long as A_{UC} is a non-constant random variable, then $\text{Cov}(A, A_{UC}) \neq 0$. Second, A_{UC} is *exogenous*, in the sense that $\epsilon \perp A_{UC}$ by Assumption 4. Third, A_{UC} obeys *exclusion restriction*. This property is implicit in the form of the outcome model imposed by Assumption 1.

Our framework distinguishes each method along two lines. First, each method implicitly makes a different assumption about the spatial scales of variation in the exposure that are correlated with the spatial error. The correlated component A_C is typically defined by two choices: 1) the type of spatial basis used, and 2) the dimension of that basis. This distinction leads to different requirements for identification of the exposure coefficient β . Ultimately, the exposure must exhibit variation that is not spanned by the spatial basis that defines A_C , i.e. the instrument A_{UC} must have nonzero variance. We label this categorization as “Property 1”.

The second criterion we use to classify spatial confounding methods in our framework is the IV approach used to leverage the instrument A_{UC} . Each of the six methods employs one of the following approaches: two-stage least squares (2SLS), where the outcome is regressed on A_{UC} ; two-stage residual inclusion (2SRI), where the outcome is regressed on both A_{UC} and A_C ; or double prediction, where the spatial variation used to construct A_C is first regressed away from the outcome, followed by regressing the resulting residuals on A_{UC} . We label this categorization as “Property 2”.

In fact, we establish the following result: under Assumptions 1-4, the coefficient estimates obtained by 2SLS, 2SRI, or double prediction are equivalent, and converge in probability to $\frac{\text{Cov}(Y, A_{UC})}{\text{Var}(A_{UC})} = \beta$. Consequently, if small-scale spatial variation in exposure is successfully extracted and uncorrelated with the spatial error, then 2SLS, 2SRI, and double prediction can each consistently recover the true parameter of interest, β . Table 1 classifies each spatial confounding method listed above within our framework, with further details available in Supplemental Section S7.

In summary, we highlight the underlying assumptions and estimation strategies that form the core of each approach by integrating existing spatial confounding literature into a unified framework. This framework reveals that each method is fundamentally driven by assumptions about which scales of variation in exposure are correlated with the spatial error, and that the uncorrelated variation corresponds to an instrumental variable. All methods assume that only large-scale spatial variability in exposure is correlated with spatial error; consequently, exposure must exhibit smaller-scale or non-spatial variation to ensure identifiability of β . However, the precise meaning of “small-scale”, “large-scale”, or “non-spatial” depends on the type and dimension of spatial basis used to decompose exposure.

Paper	Spatial basis or method used to obtain A_C	A_C	A_{UC}	Method	S_i	Analysis Model
Dupont et al. (2022)	thin-plate spline basis	$\hat{g}(S)$ (spatial)	$A - \hat{g}(S)$ (non-spatial)	2SLS	geos.	$Y_i = \beta_0 + \beta A_{UCi} + f(S_i) + \epsilon_i$, f is also obtained via a thin-plate spline with same df. as g
Urdangarin et al. (2024)	$n - k + 1$ eigenvectors of spatial precision matrix	$\sum_{i=n-k+1}^n c_i \mathbf{v}_i$ (large-scale)	$\mathbf{A} - \sum_{i=n-k+1}^n c_i \mathbf{v}_i$ (small-scale)	2SLS	areal	$Y_i \sim \text{Pois}(e_i r_i)$ $\log \mathbf{r} = \beta_0 \mathbf{1}_n + \beta \mathbf{A}_{UC} + \theta$, $\theta \sim \mathcal{N}(\mathbf{0}, \mathbf{\Omega})$, $\mathbf{\Omega}$ is a spatial precision matrix
Keller and Szpiro (2020) (preadjustment of exposure)	TPS/Fourier/Wavelet basis of dimension m , \mathbf{H}_m	$\mathbf{H}_m (\mathbf{H}_m^T \mathbf{H}_m)^{-1} \mathbf{H}_m^T \mathbf{A}$ (large-scale)	$\mathbf{A} - \mathbf{H}_m (\mathbf{H}_m^T \mathbf{H}_m)^{-1} \mathbf{H}_m^T \mathbf{A}$ (small-scale)	2SRI	geos.	$Y_i = \beta_0 + \gamma A_{Ci} + \beta A_{UCi} + \epsilon_i$
Guan et al. (2022) (semi-parametric discrete-space)	$n - 1$ eigenvectors of the Graph Laplacian	$\sum_{i=1}^{n-1} \lambda_i \mathbf{v}_i \mathbf{v}_i^T \mathbf{A}$ (large-scale)	$\lambda_n \mathbf{v}_n \mathbf{v}_n^T \mathbf{A}$ (small-scale)	2SRI	areal	$\mathbf{Y} = \beta_0$ $+ \sum_{k=1}^n (\mathbf{v}_k \mathbf{v}_k^T \mathbf{A} \sum_{l=1}^L B_l(\omega_k) b_l)$ $+ \text{CAR}(0, \sigma_z^2, \lambda_z) + \epsilon$ $B_l(\omega_k)$ are spline basis functions. $\hat{\beta} = \sum_{l=1}^L B_l(\omega_n) \hat{b}_l$.
Thaden and Kneib (2018)	Indicators for d regions $\mathbf{z}_1, \dots, \mathbf{z}_d$	$\sum_{k=1}^d \mathbf{z}_k \gamma_{1k}$ (spatial)	$\mathbf{A} - \sum_{k=1}^d \mathbf{z}_k \gamma_{1k}$ (non-spatial)	double pred.	areal	$Y_i - \sum_{k=1}^d z_{ki} \gamma_{2k}$ $= \beta [A_i - \sum_{k=1}^d z_{ki} \gamma_{1k}] + \epsilon_i$
Wiecha and Reich (2024)	universal kriging	$\hat{g}(S)$ (spatial)	$A - \hat{g}(S)$ (non-spatial)	double pred.	geos.	$A_i = g(S_i) + \epsilon_i^A$ $Y_i = \beta A_i + f(S_i) + \epsilon_i^Y$ $\hat{\beta} = ([\mathbf{A} - \hat{g}(\mathbf{S})]^T \mathbf{A})^{-1}$ $[\mathbf{A} - \hat{g}(\mathbf{S})]^T (\mathbf{Y} - \hat{f}(\mathbf{S}))$ \hat{f} is also obtained via universal kriging

Table 1: Our framework classifies each method according to two properties. The first property is the implicit assumption regarding which spatial scales of variation in exposure are correlated with the spatial error. The correlated component A_C is typically defined by some number of largest-scale elements of a spatial basis. The remaining variation in exposure, A_{UC} , is assumed to be uncorrelated with the spatial error and corresponds to an instrument. To ensure identifiability of β , the exposure must exhibit variation that is not spanned by the spatial basis that defines A_C . The second property is IV method used to leverage this decomposition and ultimately estimate β : either 1) two-stage least squares (2SLS), where an estimate of A_{UC} is substituted for exposure in the outcome regression, 2) two-stage residual inclusion (2SRI), where an estimate of A_C is included as an additional covariate in the outcome regression, or 3) double prediction or double machine learning (double pred.), where residuals of a regression of outcome on its confounded variation are regressed on residuals of a regression of exposure on A_C . Other columns of this table are defined as follows. (1) ‘‘Analysis model’’ describes the model that is used to analyze the observed data. (4) ‘‘Spatial basis used to obtain A_C ’’ refers to the basis used to decompose exposure into $A = A_C + A_{UC}$. (5) S_i denotes whether the method was originally constructed for areal or geostatistical spatial data.

3 Estimating Nonlinear Exposure-Response Curves under Spatial Confounding using IVs

In this section, we build on the IV approach introduced by Imbens and Newey (2009) to introduce the set of conditions sufficient to identify and estimate a potentially nonlinear exposure-response curve (ERC) using an instrument in the presence of unmeasured confounding. We adapt this theory slightly to fit our specific setting; see supplemental Section S8 for further details on these adaptations.

Let $\mathbf{A} = (A_1, \dots, A_n)^T \in \mathbb{R}^n$, $\mathbf{Y} = (Y_1, \dots, Y_n)^T \in \mathbb{R}^n$, $\mathbf{X} = (\mathbf{X}_1, \dots, \mathbf{X}_n)^T \in \mathbb{R}^{n \times p_1}$, $\mathbf{U} = (\mathbf{U}_1, \dots, \mathbf{U}_n)^T \in \mathbb{R}^{n \times p_2}$, denote exposure, response, measured confounders, and unmeasured confounders, respectively, measured for n units with the corresponding spatial coordinates S_1, \dots, S_n . We introduce here a scalar exposure and outcome but allow for an arbitrary number of measured and unmeasured confounders. Our target of estimation is the ERC, $\psi(a) = \mathbb{E}(Y_i(a))$, for each $a \in \mathcal{A}$ for a predefined set \mathcal{A} . This estimand is equal to the average outcome in the population if every unit were to receive exposure a . We introduce four assumptions that guarantee the identification of the ERC:

Assumption 5 (Consistency). $Y_i = Y_i(A_i)$.

Assumption 6 (Unspecified outcome model). $Y_i(a) = m(a, \mathbf{X}_i, \mathbf{U}_i)$.

Assumption 7 (Additive decomposition of exposure). $A_i = A_{UC_i} + A_{C_i}$ for some random variables $\mathbf{A}_C = (A_{C_1}, \dots, A_{C_n})^T$, $\mathbf{A}_{UC} = (A_{UC_1}, \dots, A_{UC_n})^T$.

Assumption 8 (Conditional independence of instrument). $A_{UC_i} \perp\!\!\!\perp (\mathbf{U}_i, A_{C_i}) | \mathbf{X}_i$.

Assumptions 5-8 are encoded in a causal graph in Figure 1. Assumption 5 is consistency. While we acknowledge that spatial interference is a prevalent and challenging problem in spatial causal inference (Papadogeorgou and Samanta, 2023; Reich et al., 2021), Assumption 5 implies the absence of interference, i.e. we assume that unit i 's outcome is only affected by unit i 's treatment. Assumption 6 is the form of the outcome model. Here, m is an arbitrary fixed function, and $\mathbf{X}_i, \mathbf{U}_i$ may capture any number of measured and unmeasured confounders, as well as exogeneous error, so the outcome model is left completely general.

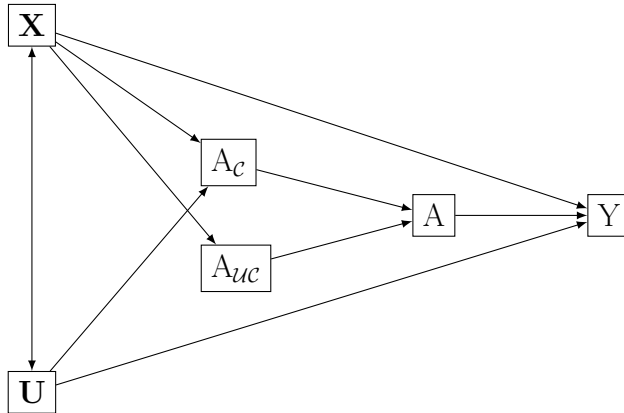


Figure 1: Causal graph illustrating assumptions. We are interested in a causal estimand describing the effect of A on Y . Our assumptions ensure that $A \perp\!\!\!\perp \mathbf{U} | (\mathbf{X}, A_C)$ implying $Y(a) \perp\!\!\!\perp A | (\mathbf{X}, A_C)$.

Assumptions 7-8 describe the generation of exposure. These assumptions posit that there exist two scalar random variables, A_C and A_{UC} , that add to form exposure A . Assumption 8, arguably the most important assumption, requires A_{UC} to be jointly independent of unmeasured confounders and the variable A_C conditional on measured confounders \mathbf{X} . A_{UC} is an instrument, since it is *relevant* (Assumption 7), *exogenous* (Assumption 8), and obeys *exclusion-restriction* (Assumption 6) conditional on measured confounders \mathbf{X} .

Given Assumptions 5-8, the following results hold:

Proposition 1 (Independence of exposure and unmeasured confounders given (\mathbf{X}, A_C)). $A_i \perp\!\!\!\perp U_i | (\mathbf{X}_i, A_{C_i})$.

Proposition 2 (Conditional ignorability given \mathbf{X}, A_C). $Y_i(a) \perp\!\!\!\perp A_i | (\mathbf{X}_i, A_{C_i}) \forall a \in \text{supp}(A)$.

Proposition 3 (Identification of ERC). *The exposure-response curve can be identified on a set of exposure values for which positivity is satisfied. Specifically, for $a \in \{a' : \text{supp}(A_C, \mathbf{X}) = \text{supp}(A_C, \mathbf{X} | A = a')\}$,*

$$\mathbb{E}(Y_i(a)) = \int \mathbb{E}(Y_i | A_i = a, A_{C_i} = a_c, \mathbf{X}_i = \mathbf{x}) dF_{A_C, \mathbf{X}}(a_c, \mathbf{x}).$$

Proposition 1 asserts that A is independent of unmeasured confounders given A_C and measured confounders \mathbf{X} . A_C . Proposition 2 asserts that conditional ignorability holds, conditional on measured confounders \mathbf{X} and the variable A_C . Finally, Proposition 3 establishes that the ERC can be identified on the set of exposure values a where $\text{supp}(A_C, \mathbf{X}) = \text{supp}(A_C, \mathbf{X} | A = a)$. Even in the presence of positivity violations, this result implies that the ERC remains identifiable on a restricted set of exposure values for which the measured confounders and A_C span the same range as in the overall population.

Assumptions 5-8 generalize the restrictive underlying assumptions of the spatial confounding methods of Section 2 (Assumptions 1-4) in the following ways. First, the dimensions of \mathbf{X} and \mathbf{U} can be arbitrary. Second, the outcome model m is no longer required to be a linear function, and instead can accommodate considerable complexity, such as nonlinearity in exposure and effect heterogeneity by measured and unmeasured confounders. For instance, m may include arbitrary interactions between nonlinear functions of A , \mathbf{U} , and \mathbf{X} . In these two ways, we have relaxed the restrictive assumptions of the spatial confounding methods of Section 2. However, we impose a stronger condition on the instrument A_{UC} than Assumptions 3-4. Instead of demanding A_{UC} to be merely uncorrelated with both \mathbf{U} and A_C , we require A_{UC} to be *jointly independent* of (\mathbf{U}, A_C) conditional on measured confounders. Caution should be exercised when applying this assumption, especially in environmental epidemiology applications; we discuss this further in Section 6.

We briefly contrast our identification strategy with other approaches for addressing unmeasured spatial confounding. Gilbert et al. (2021) require that the unmeasured confounder is a measurable function of spatial coordinates and that exposure exhibits non-spatial variation. Similarly, distance adjusted propensity score matching is justified by these same assumptions (Papadogeorgou et al., 2019). Schnell and Papadogeorgou (2020) impose strong parametric assumptions on the joint distribution of the unmeasured confounder and exposure. In contrast, our identification relies on an additive decomposition of exposure, where one component is independent of the unmeasured confounder conditional on the measured covariates. Thus, our assumptions focus more on the mechanism that generates exposure than on the behavior of the unmeasured spatial confounder. These two perspectives are closely related, but in practice, one set of assumptions may seem more plausible than the other. Does the practitioner believe that the unmeasured confounders are continuous

functions of space, or do they have strong prior knowledge about the exposure generation process, such as the presence of small-scale, localized variation that is independent of the confounders?

In the following two sections, we consider two options for the instrument A_{UC} . The first obtains A_{UC} as the residuals of a thin plate spline regression of exposure on the latitude and longitude coordinates, following (Dupont et al., 2022). The second obtains A_{UC} as the projection of exposure onto high-frequency, localized eigenvectors of the Graph Laplacian, following (Guan et al., 2022; Urdangarin et al., 2024). For estimation of the ERC, now adjusting for A_C as a covariate, we apply the methodology by Kennedy et al. (2017) using the `npcausal` package. This approach finds a doubly robust mapping whose conditional expectation under exposure equals the causal estimand, as long as either the conditional exposure density or outcome model is correctly specified.

4 Simulation

Using the spatial structure of US counties, we create datasets subject to an unmeasured spatial confounder that affects both exposure and outcome. Our proposed methodology addresses unmeasured spatial confounding bias by leveraging localized spatial variation in exposure as an instrument. The objective of the simulations are two-fold. First, we wish to evaluate the performance of our approach while varying the complexity of the outcome model. Second, we wish to investigate the performance of our approach under three different confounding mechanisms that vary the spatial scale and structure of the unmeasured spatial confounding.

We access the U.S. Census Bureau 2010 TIGER/Line Shapefiles to obtain spatial coordinates of county centroids in the contiguous United States. We restrict our simulation to the $n = 503$ counties in the sixth Environmental Protection Agency region (New Mexico, Texas, Oklahoma, Arkansas, and Louisiana) to reduce the burden of computation. For $i = 1, \dots, n = 503$, we generate (A_{UC}, A_C, U) using three different mechanisms, varying the scale or structure of the unmeasured spatial confounding. Following Paciorek (2010), all three confounding mechanisms generate (A_{UC}, A_C, U) using Gaussian processes with Matérn spatial correlation functions $R(\theta, \nu = 2)$, where distance is measured in units of 10^6 m. The first mechanism generates:

$$\begin{pmatrix} A_{UC} \\ A_C \\ U \end{pmatrix} \sim \mathcal{N} \left[\begin{pmatrix} \mathbf{0.1} \\ -\mathbf{0.2} \\ \mathbf{0.3} \end{pmatrix}, \begin{pmatrix} \mathbf{R}(\theta_{A_{UC}}) & \mathbf{0} & \mathbf{0} \\ \mathbf{0} & \mathbf{R}(\theta_{A_C}) & 0.95\mathbf{R}(\theta_{A_C}) \\ \mathbf{0} & 0.95\mathbf{R}(\theta_{A_C}) & \mathbf{R}(\theta_c) \end{pmatrix} \right],$$

with $\theta_{A_{UC}} = 0.05$ and $\theta_{A_C} = 0.5$, so that the spatial range or scale of the unconfounded component of exposure is much smaller than that of the confounded component. The second confounding mechanism is the same as the first except $\theta_{A_{UC}} = 0.1$. The third confounding mechanism uses the same Gaussian process as the first, applied independently across states. This represents an unmeasured spatial confounder that is continuous within states but discontinuous between them. For example, if A is air pollution, an unmeasured confounder could be healthcare access, which may vary smoothly within a state but shift abruptly at state borders due to differing policies or funding. Finally, exposure A is generated as $A = A_{UC} + A_C$. By design, each confounding mechanism satisfies Assumptions 7-8 of Section 3. Supplemental Section S10 contains a plot of one observation of $(A_{UC}, A_C, U)^T$ for each of the three confounding mechanisms.

We consider two possible outcome models. The linear outcome model generates outcome as $Y_i = \mathcal{N}(2U_i + A_i - 0.2A_iU_i, 1)$. The nonlinear outcome model generates outcome as $Y_i = \mathcal{N}(2U_i + A_i - 0.2A_iU_i - 0.1A_i^2 + 0.05A_i^2U_i, 1)$. For each of the 6 data-generating scenarios produced by the three confounding mechanisms and two outcome models, we create $M = 100$ datasets of size $n = 503$.

Under each data-generating scenario, we flexibly estimate the ERC using doubly-robust estimation (Kennedy et al., 2017) with four different confounding adjustment sets. The first approach (*no confounding adjustment*) does not adjust for any confounders. The second approach (*spatial coordinates*) adjusts for latitude and longitude, following Gilbert et al. (2021). The third and fourth approaches represent our proposed methodology, decomposing exposure into small- and large-scale variation, such that the small-scale variation attempts to approximate the true instrument, and the large-scale variation is adjusted for as a measured confounder. Specifically, the third approach (*IV-TPS*) fits an unpenalized thin plate spline regression of exposure on latitude and longitude with 100 degrees of freedom, and adjusts for the predicted values from this regression, drawing on Dupont et al. (2022); Keller and Szpiro (2020). The fourth approach (*IV-GraphLaplacian*) adjusts for the projection of exposure onto the smoothest 100 eigenvectors of the Graph Laplacian, corresponding to the 100 lowest eigenvalues, drawing on Guan et al. (2022); Urdangarin et al. (2024). The choice of dimension $\lfloor 0.2n \rfloor = 100$ is motivated by recommendations from Urdangarin et al. (2023).

We assess the performance of the four approaches in estimating the ERC using two key metrics: absolute bias and root mean square error (RMSE). Let $\hat{\mu}_j$ denote the estimate of the exposure-response curve in the j th simulation, $j = 1, \dots, 100$. We define average absolute bias as

$$\frac{1}{100} \sum_{i=1}^{100} \left| \frac{1}{100} \sum_{j=1}^{100} (\hat{\mu}_j(a_i) - \mu(a_i)) \right|$$

and average RMSE as

$$\frac{1}{100} \sum_{i=1}^{100} \sqrt{\frac{1}{100} \sum_{j=1}^{100} (\hat{\mu}_j(a_i) - \mu(a_i))^2}.$$

These metrics were computed as averages over 100 equally spaced exposure values in the range $[-2, 2]$. We report the values of these metrics for each method and data-generating scenario in Table 2. In general, we observe that the three approaches *IV-GraphLaplacian*, *IV-TPS*, and *spatial coordinates*, perform very similarly. They each provide approximately unbiased estimates of the true ERC, unlike the *no confounding adjustment* approach. We find that *spatial coordinates* produces estimates with slightly smaller uncertainty than *IV-GraphLaplacian* and *IV-TPS*, but encounters larger bias in the third confounding mechanism case. All simulation code can be found at <https://github.com/NSAPH-Projects/spatial-scale-confounding>.

Adjusting for spatial coordinates can adequately mitigate unmeasured spatial confounding when the confounder is a measurable function of spatial coordinates (Gilbert et al., 2021). While this assumption is not strictly satisfied by any of the confounding mechanisms considered, *spatial coordinates* remains approximately unbiased in the first two data-generating scenarios. In contrast, the third confounding mechanism deviates more significantly from this assumption, resulting in slightly larger bias for *spatial coordinates*.

The validity of *IV-TPS* and *IV-GraphLaplacian* hinges on their ability to isolate variation in exposure that is truly independent of the unmeasured confounder. Although the exposure is designed to consist of a small-scale, unconfounded component and a large-scale, confounded component, it is notable that these methods remain approximately unbiased across all data-generating scenarios, despite the fact that the data were generated using a Gaussian process rather than thin plate spline or Graph Laplacian bases.

Our simulations focus on evaluating the validity of these approaches and comparing them with state-of-the-art methods, such as Gilbert et al. (2021), under Assumptions 5-8. Future work should explore the sensitivity of these results to various modeling choices, particularly the number of basis

Confounding Mechanism	Outcome Model	No confounding adjustment	IV-GraphLaplacian	IV-TPS	Spatial Coordinates
Average Absolute Bias					
1	linear	0.766	0.132	0.129	0.144
1	nonlinear	0.822	0.122	0.118	0.181
2	linear	0.769	0.107	0.123	0.163
2	nonlinear	0.829	0.123	0.144	0.196
3	linear	0.882	0.164	0.151	0.268
3	nonlinear	0.948	0.223	0.213	0.316
Average RMSE					
1	linear	1.146	1.041	1.068	1.006
1	nonlinear	1.210	1.059	1.071	1.044
2	linear	1.153	1.084	1.087	0.996
2	nonlinear	1.225	1.079	1.124	1.038
3	linear	1.080	0.802	0.796	0.794
3	nonlinear	1.161	0.830	0.827	0.839

Table 2: Average absolute bias and average RMSE for each of the six data-generating scenarios. We consider four approaches: 1) *no confounding adjustment* does not adjust for any confounders; 2) *spatial coordinates* adjusts for latitude and longitude; 3) *IV-TPS* fits an unpenalized thin plate spline regression of exposure on latitude and longitude with 100 degrees of freedom, and adjusts for the predicted values from this regression; 4) *IV-GraphLaplacian* adjusts for the projection of exposure onto the smoothest 100 eigenvectors of the Graph Laplacian. The latter two approaches implement our proposed methodology, leveraging localized, small-scale variation in exposure as an instrument.

elements in the thin plate spline regression and Graph Laplacian projection. The basis dimension presents a bias-variance tradeoff: increasing the dimension removes large-scale spatial variation in exposure, potentially isolating unconfounded variation and producing an unbiased causal estimate, but at the cost of increased variance (Dominici et al., 2004). A potential area for future research is developing a selection procedure for the basis dimension, akin to Keller and Szpiro (2020), but without requiring parametric assumptions and for more general estimands.

5 Exposure to Air Pollution and All-Cause Mortality

In this section, we estimate the exposure-response curve between long-term average air pollution and all-cause mortality for zip codes in the contiguous United States. By intentionally excluding important spatially structured confounders, we aim to determine whether the methods introduced in the previous section can effectively adjust for unmeasured spatial confounding and recover the original ERC. The exposure A is average fine particulate matter ($PM_{2.5}$) over the period 2001-2013 estimated at the $1\text{km} \times 1\text{km}$ grid-level (Di et al., 2019), and the outcome Y is all-cause mortality rate among 68.5 million Medicare enrollees (≥ 65 years of age) over the period 2014-2016. Both exposure and outcome are aggregated to the zip code-level ($n = 33,454$). We additionally consider $p_1 = 18$ zip code-level covariates measured in 2000, including sociodemographic variables collected from the U.S. Census, American Community Survey, and the CDC’s Behavioral Risk Factor Surveillance System, as well as four meteorological variables from Gridmet via Google Earth Engine and four indicator variables for geographic region. For additional details on the data and data sources, see

Table 3.

	Variables	Mean(sd)	Data Source
Exposure	Long-term average to PM _{2.5} during 2001-2013 ($\mu\text{g}/\text{m}^3$)	10.105 (2.723)	Daily estimates of PM _{2.5} at the 1km \times 1km grid level obtained from a machine learning model combining ground, satellite and reanalysis data and subsequently aggregated to zip code-level using area-weighting (Di et al., 2017)
Outcome	All-cause mortality rate among Medicare enrollees age ≥ 65 during 2014-2016 (1/years)	0.044 (0.025)	Medicare claims data, obtained from the Centers for Medicare and Medicaid Services
Measured confounders	proportion of Hispanic residents	0.073 (0.145)	U.S. Decennial Census, American Community Survey
	proportion of Black residents	0.086 (0.167)	
	median household income (\$)	41073.934 (17090.874)	
	median home value (\$)	112053.118 (90644.856)	
	proportion of residents in poverty	0.111 (0.104)	
	proportion of residents with a high school diploma	0.378 (0.188)	
	population density (people/mi ²)	1445.148 (4682.996)	
	proportion of residents that own their house	0.731 (0.170)	
	average body mass index	26.924 (1.104)	Centers for Disease Control and Prevention’s Behavioral Risk
	proportion of smokers	0.482 (0.075)	
	average maximum daily temperature in summer (K)	301.943 (3.905)	Factor Surveillance System gridMET via Google Earth Engine
	average maximum daily temperature in winter (K)	282.132 (6.824)	
	average relative humidity in summer (%)	91.084 (10.274)	
	average relative humidity in winter (%)	86.882 (8.029)	
Midwest region	0.267 (0.442)	U.S. Census Bureau	
Northeast region	0.196 (0.397)		
South region	0.366 (0.482)		
West region	0.171 (0.377)		

Table 3: Description of zip code-level dataset ($n = 33,454$) and data sources.

We estimate the ERC using five different confounding adjustments within the doubly-robust estimation method by (Kennedy et al., 2017). The first approach adjusts for all $p_1 = 18$ measured confounders and is referred to as the *oracle*. Assuming consistency, positivity, and ignorability (conditional on these 18 confounders), and provided that the conditional exposure density or the outcome model is correctly specified, this estimated ERC would be consistent for the true ERC subject to additional regularity conditions. The second approach excludes the four temperature and humidity variables, as well as the four region indicators, but adjusts for the remaining $p_1 = 10$ measured covariates. We refer to this approach as the *baseline*, as it represents an estimate of the

ERC subject to unmeasured spatial confounding bias. The third approach adjusts for the remaining $p_1 = 10$ measured covariates as well as spatial coordinates.

The fourth and fifth approaches, *IV-TPS* and *IV-GraphLaplacian*, implement our proposed methodology from Section 3. Both approaches extract small-scale spatial variation in air pollution as the instrument A_{UC} and adjust for the remaining large-scale spatial variation A_C alongside the remaining $p_1 = 10$ measured covariates. Due to the substantial computational burden of calculating basis elements, and given the spatially smooth nature of air pollution exposure, we chose to use bases of dimension 5. Figure 2 presents the exposure, the two candidate instrumental variables A_{UC} , and the two candidate adjustment variables A_C . Table 4 provides the correlation of each excluded spatial confounder with the exposure and two candidate IVs. Previous studies suggest that sharp spatial patterns in exposure to air pollution result from random fluctuations in wind patterns and are therefore independent of unmeasured confounders (Schwartz et al., 2017, 2018; Jayachandran, 2009; Cabral and Dillender, 2024; Bondy et al., 2020; Gu et al., 2020; Yang and Zhang, 2018). We adopt a similar assumption, hypothesizing that our two candidate instruments A_{UC} —representing localized spatial variation in air pollution exposure as shown in Figure 2—are independent of the omitted temperature, humidity, and region variables, conditional on the remaining $p_1 = 10$ measured confounders.

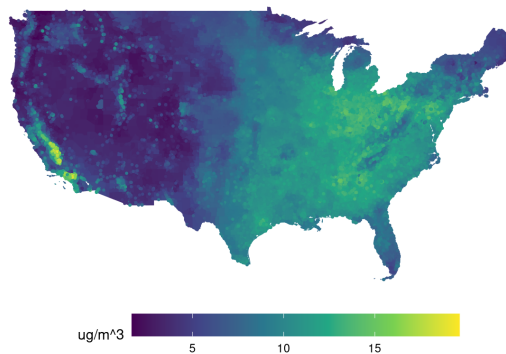
	Exposure	IV-TPS	IV-GraphLaplacian
average maximum daily summer temperature	0.17	0.12	0.15
average maximum daily winter temperature	0.17	0.10	0.22
average relative summer humidity	0.41	0.13	0.14
average relative winter humidity	-0.02	-0.05	-0.07
Midwest region	0.16	0.02	0.12
Northeast region	-0.05	0.08	0.02
South region	0.23	-0.01	-0.07
West region	-0.43	-0.08	-0.06

Table 4: Correlation of each excluded spatial confounder with exposure and the two candidate IVs.

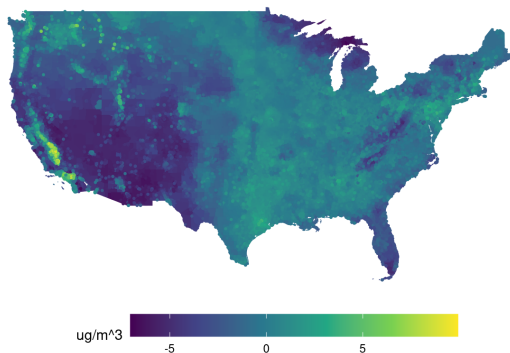
For each of the five estimation strategies, we calculate $\mathbb{E}(Y(a))$ at 100 equally spaced values of a between the minimum and maximum of the exposure distribution. The first panel of Figure 3 shows the five estimated ERCs within the percentile range (5%, 95%) of exposure. The *baseline* ERC deviates significantly from the *oracle* ERC for exposure values 10–12 $\mu\text{g}/\text{m}^3$, as the *oracle* curve falls outside the confidence interval of the *baseline*, indicating that unmeasured spatial confounding is indeed present by omitting variables of temperature, humidity and region. *IV-TPS* most effectively mitigates confounding bias, although both the *IV-TPS* and *IV-GraphLaplacian* estimates exhibit large uncertainty similar to the *oracle*. The *spatial-coordinates* method yields a biased estimate with smaller uncertainty, closely resembling the *baseline*.

We emphasize two key points. First, the bias resulting from the unmeasured spatial confounding due to the exclusion of temperature, humidity, and regional variables is small, although present throughout the range of exposure. This finding is consistent with those of Wu et al. (2020), whose sensitivity analyses indicated that point estimates do not vary much when temperature and humidity were excluded. However, artificially inducing unmeasured spatial confounding substantially influences uncertainty, as the *baseline* confidence intervals are considerably narrower than those produced by the *oracle*. Despite the wide confidence intervals associated with the *IV-TPS* and *IV-GraphLaplacian* methods, these approaches are preferable in this context due to their ability to appropriately quantify the *oracle*’s uncertainty. In contrast, the *spatial coordinates* approach

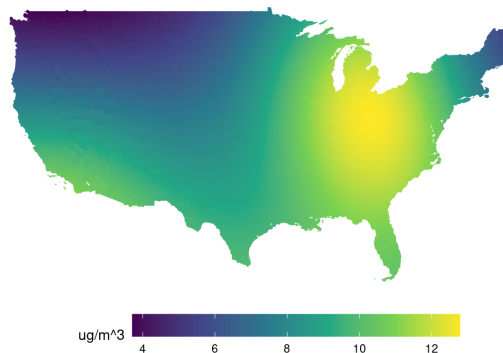
PM_{2.5} Exposure (A) averaged over 2001-2013 across US zip codes



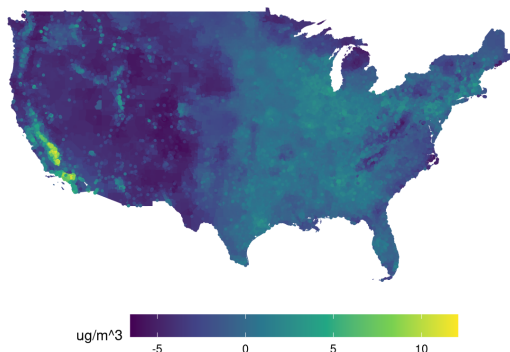
Estimate of the instrumental variable (A_{uc}) using a thin plate spline



Estimate of the adjustment variable (A_c) using a thin plate spline



Estimate of the instrumental variable (A_{uc}) using the Graph Laplacian



Estimate of the adjustment variable (A_c) using the Graph Laplacian

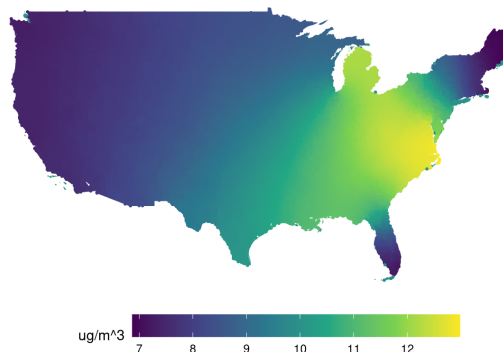


Figure 2: Long-term averaged exposure to PM_{2.5} at the zip code level during 2001-2013, two candidate IVs, and two candidate adjustment variables. The first candidate IV consists of the residuals of a regression of exposure on a thin plate spline of spatial coordinates of zip code centroids with 5 degrees of freedom. The second candidate IV consists of the residuals of a regression of exposure on the 5 eigenvectors of the Graph Laplacian corresponding to the smallest eigenvalues. Both IVs represent localized, small-scale spatial variation in exposure to air pollution. Both Post Office boxes (represented with point shapefiles) and Zip Code Tabulation Areas (represented with polygon shapefiles) are plotted above. Shapefiles sourced from ESRI, 2013.

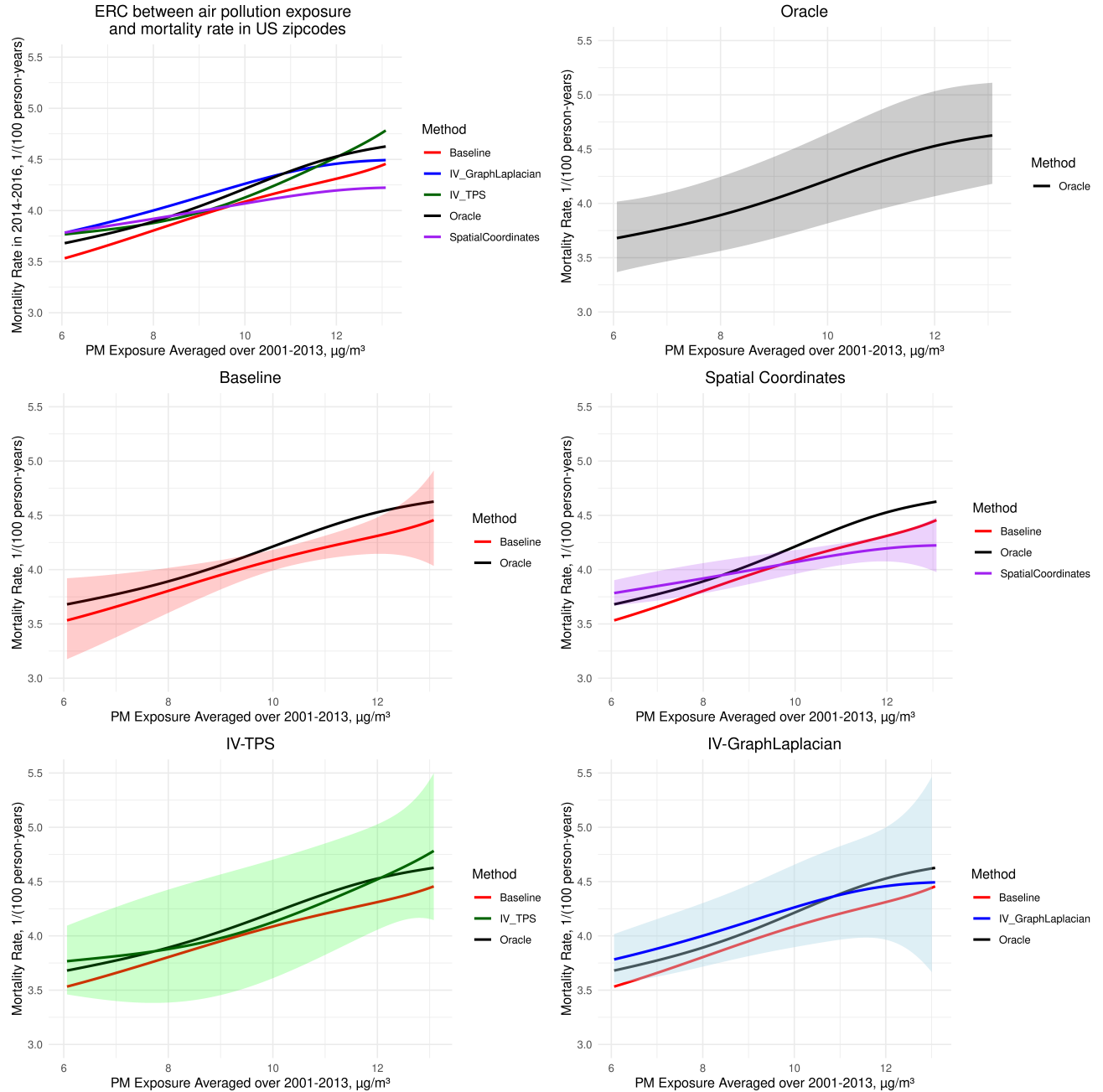


Figure 3: Estimates of the exposure-response curve between long-term exposure to $\text{PM}_{2.5}$ during 2001-2013 and all-cause mortality during 2014-2016 among Medicare enrollees using five different confounding adjustments within doubly-robust estimation: 1) the *oracle* adjusts for all 18 measured confounders; 2) the *baseline* adjusts for 10 measured confounders, excluding temperature and humidity variables, as well as region indicators; 3) *spatial coordinates* adjusts for the remaining 10 measured confounders, as well as latitude and longitude; 4) *IV-TPS* adjusts for the remaining 10 measured confounders and the predicted values from a thin plate spline regression of exposure on spatial coordinates with 5 degrees of freedom; 5) *IV-GraphLaplacian* adjusts for the remaining 10 measured confounders and the projection of exposure onto the smoothest 5 eigenvectors of the Graph Laplacian corresponding to the smallest 5 eigenvalues.

yields very narrow confidence intervals centered around the *baseline*, potentially underestimating uncertainty. However, we caution against over-interpreting these results, as the *oracle* itself may be subject to residual unmeasured confounding and may not represent an unbiased estimate of the true ERC.

Despite these differences, all estimated ERCs indicate a statistically significant harmful effect of long-term average exposure to PM_{2.5} during 2001-2013 on all-cause mortality during 2014-2016 in US zip codes. The estimated causal risk ratio $\frac{\mathbb{E}(Y(12))}{\mathbb{E}(Y(9))}$, comparing the mortality rate from 2014 to 2016 if all zip codes in the US had experienced an average PM_{2.5} exposure of $12\mu\text{g}/\text{m}^3$ (the primary annual National Ambient Air Quality Standard before 2024) versus $9\mu\text{g}/\text{m}^3$ (the revised standard) during the period 2001-2013, is approximately 1.071. This is reasonably consistent with the effect sizes reported in other studies of air pollution and mortality (Wu et al., 2020; Dockery et al., 1993; Beelen et al., 2014; Di et al., 2017; Liu et al., 2019; Pappin et al., 2019).

6 Discussion

Adjusting for unmeasured spatial confounding is critical for accurate causal inference, as failing to address confounding bias can lead to erroneous conclusions, misguided decisions, and suboptimal policy. In this paper, we argue that many existing methods for addressing spatial confounding are built on a common foundation: they assume that exposure can be decomposed additively into two components, a large-scale component, correlated with the unmeasured confounder, and an uncorrelated small-scale component. These methods then leverage the small-scale component as an instrumental variable to estimate the parameter of interest. By categorizing these methods within a unified framework, we clarify the distinct assumptions and estimation strategies employed by each. A key insight is that the interpretation of “large-scale” and “small-scale” depends critically on the type and dimension of the basis used in the exposure decomposition. This distinction is significant because assumptions about confounding may hold under one choice of basis but fail under another, affecting the validity of the method, a point also raised by Keller and Szpiro (2020).

The spatial confounding methods above are constrained by their reliance on linear outcome models and effect homogeneity. We address these limitations by adapting the methodologies of (Imbens and Newey, 2009; Kennedy et al., 2017) to nonparametrically identify and estimate causal effects, while extending key concepts from the spatial confounding methods. Specifically, we employ flexible modeling to estimate the exposure-response curve, while accounting for unmeasured spatial confounding that impacts only certain scales of variation in the exposure. Our approach builds on the methodology of (Gilbert et al., 2021) by allowing exposures to be perfectly smooth in space, provided that we can distinguish between confounded and unconfounded scales of variation in exposure.

Our approach also faces some limitations. First, identifying valid instrumental variation in environmental epidemiology is extremely challenging, and caution is needed when applying instruments in these contexts (Greenland, 2000; Weisskopf and Seals, 2015). Second, the method assumes an additive decomposition of exposure into confounded and unconfounded components, which may not always hold. This assumption can be relaxed by replacing $A = A_{UC} + A_C$ with $A = h(A_{UC}, A_C)$, where h is an unknown monotonic function in its second argument (Imbens and Newey, 2009). Third, identifying the exposure-response curve requires strong positivity, which is often violated in settings with continuous spatial data (Petersen et al., 2012). In such cases, we advocate targeting estimands that relax this assumption, such as shift estimands or incremental propensity score interventions (Gilbert et al., 2021; Schindl et al., 2024).

There are several avenues for future research. First, as discussed in Section 4, the choice of basis

type and dimension used for spatial confounding adjustment raise the need for a sensitivity analysis framework. Additionally, only a limited class of spatial confounders are continuous functions of space, while many—such as zoning regulations or healthcare access shaped by state policies—exhibit discontinuous spatial patterns. To our knowledge, no existing methodology can adjust for these types of confounders, but we believe our approach could be extended to do so by incorporating a more diverse set of spatial basis elements into the exposure decomposition. Finally, the joint consideration of unmeasured confounding with spatiotemporal data and interference remains relatively unexplored and presents another promising direction for future work.

Acknowledgments

The authors would like to thank Dr. Heejun Shin and James Kitch for their thoughtful comments. The computations in this paper were run on the FASRC Cannon cluster supported by the FAS Division of Science Research Computing Group at Harvard University.

Funding

SMW, MGT, and FD gratefully acknowledge support from the National Institutes of Health under award numbers R01ES030616, R01AG066793, RF1AG074372-01A1, R01MD016054, R01ES034373, RF1AG080948, U24ES035309, RF1AG071024, P30ES000002, R01ES34021, R01ES037156-01, T32ES007142; the Sloan Foundation G-2020-13946; and the National Science Foundation Graduate Research Fellowship under Grant No. DGE 2140743. Any opinion, findings, and conclusions or recommendations expressed in this material are those of the authors and do not necessarily reflect the views of the funders.

References

- Amemiya, T. (1974). The nonlinear two-stage least-squares estimator. *Journal of econometrics*, 2(2):105–110.
- Andrews, D. W. (1994). Asymptotics for semiparametric econometric models via stochastic equicontinuity. *Econometrica: Journal of the Econometric Society*, pages 43–72.
- Angrist, J. and Imbens, G. (1995). Identification and estimation of local average treatment effects.
- Angrist, J. D., Imbens, G. W., and Rubin, D. B. (1996). Identification of causal effects using instrumental variables. *Journal of the American statistical Association*, 91(434):444–455.
- Baiocchi, M., Cheng, J., and Small, D. S. (2014). Instrumental variable methods for causal inference. *Statistics in medicine*, 33(13):2297–2340.
- Beelen, R., Raaschou-Nielsen, O., Stafoggia, M., Andersen, Z. J., Weinmayr, G., Hoffmann, B., Wolf, K., Samoli, E., Fischer, P., Nieuwenhuijsen, M., et al. (2014). Effects of long-term exposure to air pollution on natural-cause mortality: an analysis of 22 european cohorts within the multicentre escape project. *The lancet*, 383(9919):785–795.
- Bobb, J. F., Cruz, M. F., Mooney, S. J., Drewnowski, A., Arterburn, D., and Cook, A. J. (2022). Accounting for spatial confounding in epidemiological studies with individual-level exposures: An exposure-penalized spline approach. *Journal of the Royal Statistical Society Series A: Statistics in Society*, 185(3):1271–1293.

- Bondy, M., Roth, S., and Sager, L. (2020). Crime is in the air: The contemporaneous relationship between air pollution and crime. *Journal of the Association of Environmental and Resource Economists*, 7(3):555–585.
- Cabral, M. and Dillender, M. (2024). Air pollution, wildfire smoke, and worker health. Technical report, National Bureau of Economic Research.
- Chernozhukov, V., Chetverikov, D., Demirer, M., Duflo, E., Hansen, C., Newey, W., and Robins, J. (2018). Double/debiased machine learning for treatment and structural parameters.
- Di, Q., Amini, H., Shi, L., Kloog, I., Silvern, R., Kelly, J., Sabath, M. B., Choirat, C., Koutrakis, P., Lyapustin, A., et al. (2019). An ensemble-based model of pm_{2.5} concentration across the contiguous united states with high spatiotemporal resolution. *Environment international*, 130:104909.
- Di, Q., Wang, Y., Zanobetti, A., Wang, Y., Koutrakis, P., Choirat, C., Dominici, F., and Schwartz, J. D. (2017). Air pollution and mortality in the medicare population. *New England Journal of Medicine*, 376(26):2513–2522.
- Dockery, D. W., Pope, C. A., Xu, X., Spengler, J. D., Ware, J. H., Fay, M. E., Ferris Jr, B. G., and Speizer, F. E. (1993). An association between air pollution and mortality in six us cities. *New England journal of medicine*, 329(24):1753–1759.
- Dominici, F., McDermott, A., and Hastie, T. J. (2004). Improved semiparametric time series models of air pollution and mortality. *Journal of the American Statistical Association*, 99(468):938–948.
- Dupont, E., Marques, I., and Kneib, T. (2023). Demystifying spatial confounding. *arXiv preprint arXiv:2309.16861*.
- Dupont, E., Wood, S., and Augustin, N. (2022). Spatial+: a novel approach to spatial confounding. *Biometrics*.
- Fewell, Z., Davey Smith, G., and Sterne, J. A. (2007). The impact of residual and unmeasured confounding in epidemiologic studies: a simulation study. *American journal of epidemiology*, 166(6):646–655.
- Giffin, A., Reich, B. J., Yang, S., and Rappold, A. G. (2021). Instrumental variables, spatial confounding and interference. *arXiv preprint arXiv:2103.00304*.
- Gilbert, B., Datta, A., Casey, J. A., and Ogburn, E. L. (2021). A causal inference framework for spatial confounding. *arXiv preprint arXiv:2112.14946*.
- Greene, W. H. (2003). *Econometric analysis*. Pearson Education India.
- Greenland, S. (2000). An introduction to instrumental variables for epidemiologists. *International journal of epidemiology*, 29(4):722–729.
- Gu, H., Yan, W., Elahi, E., and Cao, Y. (2020). Air pollution risks human mental health: an implication of two-stages least squares estimation of interaction effects. *Environmental Science and Pollution Research*, 27(2):2036–2043.
- Guan, Y., Page, G. L., Reich, B. J., Ventrucci, M., and Yang, S. (2022). Spectral adjustment for spatial confounding. *Biometrika*, page asac069.

- Hanks, E. M., Schliep, E. M., Hooten, M. B., and Hoeting, J. A. (2015). Restricted spatial regression in practice: geostatistical models, confounding, and robustness under model misspecification. *Environmetrics*, 26(4):243–254.
- Hausman, J. A. (1978). Specification tests in econometrics. *Econometrica: Journal of the econometric society*, pages 1251–1271.
- Imbens, G. (2014). Instrumental variables: An econometrician’s perspective. Technical report, National Bureau of Economic Research.
- Imbens, G. W. and Newey, W. K. (2009). Identification and estimation of triangular simultaneous equations models without additivity. *Econometrica*, 77(5):1481–1512.
- Jayachandran, S. (2009). Air quality and early-life mortality: Evidence from indonesia’s wildfires. *Journal of Human resources*, 44(4):916–954.
- Keller, J. and Szpiro, A. (2020). Selecting a scale for spatial confounding adjustment. *Journal of the Royal Statistical Society: Series A (Statistics in Society)*, 183(3):1121–1143.
- Kennedy, E. H., Ma, Z., McHugh, M. D., and Small, D. S. (2017). Non-parametric methods for doubly robust estimation of continuous treatment effects. *Journal of the Royal Statistical Society Series B: Statistical Methodology*, 79(4):1229–1245.
- Khan, K. and Berrett, C. (2023). Re-thinking spatial confounding in spatial linear mixed models. *arXiv preprint arXiv:2301.05743*.
- Liu, C., Chen, R., Sera, F., Vicedo-Cabrera, A. M., Guo, Y., Tong, S., Coelho, M. S., Saldiva, P. H., Lavigne, E., Matus, P., et al. (2019). Ambient particulate air pollution and daily mortality in 652 cities. *New England Journal of Medicine*, 381(8):705–715.
- Nobre, W. S., Schmidt, A. M., and Pereira, J. B. (2021). On the effects of spatial confounding in hierarchical models. *International Statistical Review*, 89(2):302–322.
- Paciorek, C. (2010). The importance of scale for spatial-confounding bias and precision of spatial regression estimators. *Statistical Science*, 25:107 – 125.
- Papadogeorgou, G., Choirat, C., and Zigler, C. (2019). Adjusting for unmeasured spatial confounding with distance adjusted propensity score matching. *Biostatistics*, 20(2):256–272.
- Papadogeorgou, G. and Samanta, S. (2023). Spatial causal inference in the presence of unmeasured confounding and interference. *arXiv preprint arXiv:2303.08218*.
- Pappin, A. J., Christidis, T., Pinault, L. L., Crouse, D. L., Brook, J. R., Erickson, A., Hystad, P., Li, C., Martin, R. V., Meng, J., et al. (2019). Examining the shape of the association between low levels of fine particulate matter and mortality across three cycles of the canadian census health and environment cohort. *Environmental health perspectives*, 127(10):107008.
- Pearce, N., Vandenbroucke, J. P., and Lawlor, D. A. (2019). Causal inference in environmental epidemiology: old and new approaches. *Epidemiology*, 30(3):311–316.
- Petersen, M. L., Porter, K. E., Gruber, S., Wang, Y., and Van Der Laan, M. J. (2012). Diagnosing and responding to violations in the positivity assumption. *Statistical methods in medical research*, 21(1):31–54.

- Reich, B., Yang, S., Guan, Y., Giffin, A., Miller, M., and Rappold, A. (2021). A review of spatial causal inference methods for environmental and epidemiological applications. *International Statistical Review*, 89(3):605–634.
- Robins, J. M., Rotnitzky, A., and Scharfstein, D. O. (2000). Sensitivity analysis for selection bias and unmeasured confounding in missing data and causal inference models. In *Statistical models in epidemiology, the environment, and clinical trials*, pages 1–94. Springer.
- Robinson, P. M. (1988). Root-n-consistent semiparametric regression. *Econometrica: Journal of the Econometric Society*, pages 931–954.
- Rothman, K. J. and Greenland, S. (2005). Causation and causal inference in epidemiology. *American journal of public health*, 95(S1):S144–S150.
- Schindl, K., Shen, S., and Kennedy, E. H. (2024). Incremental effects for continuous exposures. *arXiv preprint arXiv:2409.11967*.
- Schnell, P. and Papadogeorgou, G. (2020). Mitigating unobserved spatial confounding when estimating the effect of supermarket access on cardiovascular disease deaths. *The Annals of Applied Statistics*, 14(4):2069–2095.
- Schwartz, J., Bind, M.-A., and Koutrakis, P. (2017). Estimating causal effects of local air pollution on daily deaths: effect of low levels. *Environmental health perspectives*, 125(1):23–29.
- Schwartz, J., Fong, K., and Zanobetti, A. (2018). A national multicity analysis of the causal effect of local pollution, no 2, and pm 2.5 on mortality. *Environmental health perspectives*, 126(8):087004.
- Tec, M., Trisovic, A., Audirac, M., Woodward, S., Hu, J., Khoshnevis, N., and Dominici, F. (2024). Space: The spatial confounding environment. In *Proceedings of the International Conference on Learning Representations (ICLR)*. ICLR.
- Terza, J. V., Basu, A., and Rathouz, P. J. (2008). Two-stage residual inclusion estimation: addressing endogeneity in health econometric modeling. *Journal of health economics*, 27(3):531–543.
- Thaden, H. and Kneib, T. (2018). Structural equation models for dealing with spatial confounding. *The American Statistician*, 72(3):239–252.
- Urdangarin, A., Goicoa, T., Kneib, T., and Ugarte, M. D. (2024). A simplified spatial+ approach to mitigate spatial confounding in multivariate spatial areal models. *Spatial Statistics*, 59:100804.
- Urdangarin, A., Goicoa, T., and Ugarte, M. D. (2023). Evaluating recent methods to overcome spatial confounding. *Revista Matemática Complutense*, 36(2):333–360.
- VanderWeele, T. J. and Arah, O. A. (2011). Bias formulas for sensitivity analysis of unmeasured confounding for general outcomes, treatments, and confounders. *Epidemiology*, 22(1):42–52.
- Weisskopf, M. G. and Seals, R. M. (2015). Instrumental variables and the trouble with analyses of mixtures. In *ISEE Conference Abstracts 27*, volume 2015, page 890.
- Wiecha, N. and Reich, B. J. (2024). Two-stage spatial regression models for spatial confounding. *arXiv preprint arXiv:2404.09358*.
- Wright, P. G. (1928). *The tariff on animal and vegetable oils*. Number 26. Macmillan.

Wu, X., Braun, D., Schwartz, J., Kioumourtzoglou, M., and Dominici, F. (2020). Evaluating the impact of long-term exposure to fine particulate matter on mortality among the elderly. *Science advances*, 6(29):eaba5692.

Yang, J. and Zhang, B. (2018). Air pollution and healthcare expenditure: Implication for the benefit of air pollution control in china. *Environment international*, 120:443–455.

Supporting Information

The Supplementary Material consists of three sections. In Section S7 we classify the remaining five spatial confounding methods under our IV framework. In Section S8, we provide proofs of Propositions 1-3 and describe the minor adaptations made to the theory of Imbens and Newey (2009) to suit our context. In Section S9, we outline the details of the doubly-robust estimation method as applied to our setting. Section S10 contains additional figures related to the simulation study. Code to replicate the simulation study is provided at <https://github.com/NSAPH-Projects/spatial-scale-confounding>.

S7 Unifying Six Spatial Confounding Methods Under an IV Framework

Below we classify the six spatial confounding methods (Dupont et al., 2022; Urdangarin et al., 2023; Keller and Szpiro, 2020; Guan et al., 2022; Thaden and Kneib, 2018; Wiecha and Reich, 2024) as special cases of our framework. We use the same notation as Table 1 in the main text.

2SLS Methods

Dupont et al. (2022) and Urdangarin et al. (2024) employ the instrument A_{UC} in two-stage least squares (2SLS). In the first stage, exposure is decomposed into large-scale spatial variation correlated with the spatial error (A_C) and small-scale spatial variation uncorrelated with the spatial error (A_{UC}). In the second stage, exposure is substituted with A_{UC} in an outcome regression (Baiocchi et al., 2014; Terza et al., 2008; Greene, 2003). Given that the first stage correctly identifies variation in exposure uncorrelated with the spatial error, the coefficient estimate of A_{UC} obtained from the second regression converges in probability to

$$\frac{\text{Cov}(Y, A_{UC})}{\text{Var}(A_{UC})} = \frac{\text{Cov}(\beta_0 + \beta A + \epsilon, A_{UC})}{\text{Var}(A_{UC})} = \frac{\text{Cov}(\beta A_C + \beta A_{UC} + \epsilon, A_{UC})}{\text{Var}(A_{UC})} = \beta,$$

the statistical parameter of interest. The first equality follows from assumption 1, the second equality follows from assumption 2, and the third equality follows from assumptions 3 and 4.

The spatial+ method proposed by Dupont et al. (2022), without smoothing, is an example of a 2SLS method that decomposes exposure using a **thin plate spline basis**. Specifically, the first stage fits a thin plate spline of spatial coordinates to exposure. A_C are the predicted values from this regression, $\hat{g}(S)$ while the instrument A_{UC} are the residuals, $A - \hat{g}(S)$. The second stage regresses outcome on A_{UC} and a thin plate spline of spatial coordinates with the same degrees of freedom as the first stage. Identifiability of β requires exposure to exhibit variation that is not spanned by the thin plate spline basis.

The simplified spatial+ method proposed by Urdangarin et al. (2024) is an example of a 2SLS method that decomposes exposure using the **eigenvector basis of a spatial precision matrix**. Broadly speaking, eigenvectors of a spatial precision matrix capture spatial information at different scales, with those corresponding to the lowest non-zero eigenvalues representing the smoothest spatial patterns. A_C is obtained as the projection of exposure \mathbf{A} onto the subspace spanned by k eigenvectors of the spatial precision matrix corresponding to the smallest k eigenvalues, $\sum_{i=n-k+1}^n c_i \mathbf{v}_i$ for some $\{c_i\}_{i=1}^n$, thus capturing the large-scale or smoothest spatial variation in exposure. A_{UC} is the projection of \mathbf{A} onto the remaining $n - k$ eigenvectors corresponding to the $n - k$ highest eigenvalues, $\mathbf{A} - \sum_{i=n-k+1}^n c_i \mathbf{v}_i$, thus capturing the small-scale or localized spatial

variation in exposure. The second stage regresses outcome on A_{UC} with spatial random effects. Identifiability of β requires exposure to exhibit variation in the subspace spanned by the $n - k$ small-scale eigenvectors.

2SRI Methods

Guan et al. (2022) and Section 2.3 of Keller and Szpiro (2020) use A_{UC} as an instrument in two-stage residual inclusion (2SRI). The first stage of 2SRI is identical to the first stage of 2SLS. In the second stage estimation, first-stage residuals are included as additional regressors (Terza et al., 2008; Hausman, 1978). Specifically, the outcome is regressed on both A_C and A_{UC} . The estimated coefficient of A_{UC} from the second-stage regression converges in probability to

$$\frac{\text{Var}(A_C)\text{Cov}(Y, A_{UC}) - \text{Cov}(A_{UC}, A_C)\text{Cov}(Y, A_C)}{\text{Var}(A_C)\text{Var}(A_{UC}) - (\text{Cov}(A_{UC}, A_C))^2} = \frac{\text{Cov}(Y, A_{UC})}{\text{Var}(A_{UC})} = \beta,$$

where the first equality follows by assumption 3, and the second equality follows from the 2SLS case.

The approach proposed by Keller and Szpiro (2020) (Sections 2.2-2.3) is an example of a 2SRI method. The authors suggest **choosing a type of hierarchical spatial basis \mathbf{H}** , meaning a basis whose elements are ordered by some notion of spatial scale, such as a thin plate spline basis, Fourier basis, or wavelet basis. They then propose **selecting some number of basis vectors m by minimizing AIC/BIC in a regression of outcome on the basis vectors**. In the first stage decomposition, \mathbf{A}_C is obtained as the projection of exposure \mathbf{A} onto the m largest scale vectors of the chosen basis, $\mathbf{H}_m(\mathbf{H}_m^T\mathbf{H}_m)^{-1}\mathbf{H}_m^T\mathbf{A}$, while \mathbf{A}_{UC} is obtained as the projection of \mathbf{A} onto the remaining $n - m$ smaller-scale basis vectors $\mathbf{A} - \mathbf{H}_m(\mathbf{H}_m^T\mathbf{H}_m)^{-1}\mathbf{H}_m^T\mathbf{A}$. Identifiability of β requires exposure to exhibit variation in the subspace spanned by these $n - m$ small-scale basis vectors.

The discrete-space methodology presented by Guan et al. (2022) is an example of a 2SRI method that exploits small-scale variation in exposure as the instrument using the **eigenbasis of the Graph Laplacian**. In particular, they assume that correlation between the exposure and confounder in the spectral domain diminishes as the magnitude of the spatial frequency ω increases; moreover, the correlation at the highest frequency $\alpha(\omega_n)$ is assumed to be zero. Since the eigenvectors $\mathbf{v}_1, \dots, \mathbf{v}_n$ of the Graph Laplacian are ordered by a notion of spatial scale, this implies that the correlation between confounder and exposure dissipates at small scales, and is zero at the smallest scale. The first-stage decomposition obtains $\mathbf{A}_C = \sum_{k=1}^{n-1} \lambda_k \mathbf{v}_k \mathbf{v}_k^T \mathbf{A}$ and $\mathbf{A}_{UC} = \lambda_n \mathbf{v}_n \mathbf{v}_n^T \mathbf{A}$. (More accurately, \mathbf{A}_C is a the set of vectors $\{\lambda_k \mathbf{v}_k \mathbf{v}_k^T \mathbf{A}\}_{k=1}^{n-1}$ since each of these vectors is assigned its own coefficient in the outcome regression.) Identifiability of β requires exposure to exhibit variation in the subspace spanned by the n th eigenvector of the Graph Laplacian.

Double prediction methods

Thaden and Kneib (2018); Wiecha and Reich (2024) employ A_{UC} as an instrument in double prediction. In the first stage of double prediction, both the exposure and outcome are decomposed into spatial variation correlated with the spatial error (obtaining A_C, Y_C) and spatial variation uncorrelated with the spatial error (obtaining A_{UC}, Y_{UC}). In the second stage outcome regression, Y_{UC} is regressed on A_{UC} (Robinson, 1988; Andrews, 1994; Chernozhukov et al., 2018). Given that the first-stage regression correctly identifies variation in exposure uncorrelated with the spatial error, and that Y_C is constructed such that $Y_C \perp A_{UC}$, the coefficient estimate of A_{UC} obtained

from the second regression converges in probability to

$$\frac{\text{Cov}(A_{UC}, Y_{UC})}{\text{Var}(A_{UC})} = \frac{\text{Cov}(A_{UC}, Y - Y_C)}{\text{Var}(A_{UC})} = \frac{\text{Cov}(A_{UC}, Y)}{\text{Var}(A_{UC})} = \beta,$$

where the last equality follows from the 2SLS case.

The geoaddivitive structural equation model (gSEM) proposed by Thaden and Kneib (2018) is an example of a double prediction method that exploits small-scale variation in exposure as the instrument using a **region-level indicator basis**. In the first stage of gSEM, exposure is regressed on region-level indicators $\mathbf{z}_1, \dots, \mathbf{z}_d$. \mathbf{A}_C are the predicted values from this regression $\sum_{k=1}^d \mathbf{z}_k \gamma_{1k}$ and \mathbf{A}_{UC} are the residuals $\mathbf{A} - \sum_{k=1}^d \mathbf{z}_k \gamma_{1k}$. Y_{UC} is also obtained by regressing outcome on the region-level indicators. Identifiability of β requires both exposure and outcome to exhibit variation outside of the subspace spanned by the region-level indicators.

Double spatial regression (DSR) proposed by Wiecha and Reich (2024) is an example of a double prediction method that exploits small-scale variation in exposure as the instrument using **Gaussian process regression with Matérn correlation**. In both the first and second stages of DSR, a polynomial function of spatial coordinates is fitted to the exposure and outcome, respectively, while modeling spatially autocorrelated errors with Matérn correlation. \mathbf{A}_C are the predicted values $\hat{g}(S)$ from this regression while \mathbf{A}_{UC} are the residuals $\mathbf{A} - \hat{g}(S)$. Identifiability of β requires exposure to exhibit variation beyond the polynomial trend of the spatial coordinates fit to exposure.

S8 Identification Results and Comparison with Imbens and Newey (2009)

We provide a brief comparison of our identification approach with that of Imbens and Newey (2009). Table S5 presents our assumptions and propositions in contrast to those of Imbens and Newey (2009), if their identification approach were directly applied to our setting.

	Proposed Methodology	Imbens and Newey (2009)
Assumptions	<p>A5: $Y_i = Y_i(A_i)$</p> <p>A6: $Y_i(a) = m(a, \mathbf{X}_i, \mathbf{U}_i)$</p> <p>A7: $A_i = A_{UC_i} + A_{C_i}$</p> <p>A8: $A_{UC_i} \perp\!\!\!\perp (\mathbf{U}_i, A_{C_i}) \mathbf{X}_i$</p>	<p>A6': $Y_i = m(A_i, \mathbf{U}_i)$</p> <p>A7': $A_i = h(A_{UC_i}, A_{C_i})$, h strictly monotonic in its second argument with probability 1</p> <p>A8': $A_{UC_i} \perp\!\!\!\perp (\mathbf{U}_i, A_{C_i})$</p> <p>A9': A_C is a continuously distributed scalar with CDF that is strictly increasing on its support</p>
Propositions	<p>P1: $A_i \perp\!\!\!\perp \mathbf{U}_i (\mathbf{X}_i, A_{C_i})$</p> <p>P2: $Y_i(a) \perp\!\!\!\perp A_i (\mathbf{X}_i, A_{C_i}) \forall a \in \text{supp}(A)$</p> <p>P3: $\forall a \in \{a' : \text{supp}(A_C, \mathbf{X}) = \text{supp}(A_C, \mathbf{X} A = a')\}$, $\mathbb{E}(Y_i(a)) = \mathbb{E}(\mathbb{E}(Y_i A_i = a, A_{C_i}, \mathbf{X}_i))$</p>	<p>P1': $A_i \perp\!\!\!\perp \mathbf{U}_i V_i = F_{A A_{UC}}(A_i A_{UC_i})$</p> <p>P2': $m(a, \mathbf{U}) \perp\!\!\!\perp A V$</p> <p>P3': $\forall a \in \{a' : \text{supp}(V) = \text{supp}(V A = a')\}$, $\mathbb{E}(m(a, \mathbf{U}_i)) = \mathbb{E}(\mathbb{E}(Y_i A_i = a, V_i))$</p>

Table S5: Comparison of our proposed methodology with that of Imbens and Newey (2009). To align with existing spatial confounding literature and facilitate causal inference, we introduce three modifications: (1) the use of potential outcomes notation; (2) a known, additive decomposition of exposure; and (3) additional conditioning on measured confounders.

Our methodology differs from Imbens and Newey (2009) in three ways. First, we explicitly introduce potential outcomes notation to enable causal inference. Second, Imbens and Newey (2009) relax our Assumption 7 by assuming that $A = h(A_C, A_{UC})$ for some unknown function h that is strictly monotonic in its second argument with probability 1. We instead substitute h with a simple additive function to align with the existing spatial confounding methods in the literature. Additionally, this avoids the need to estimate and adjust for $V = F_{A|A_{UC}}(A|A_{UC})$, because we can directly adjust for A_C . Consequently, A9' is no longer required.

The third distinction is the inclusion of measured confounders, \mathbf{X} , which allows us to replace the independence assumption (A8') with conditional independence (A8) of the instrument. We consider the latter to be more plausible in many contexts. The conditioning on \mathbf{X} is extended throughout the propositions, so that conditional ignorability is achieved by conditioning on both A_C and \mathbf{X} , rather than A_C alone.

Below we present the proofs of Propositions 1–3 under Assumptions 5–8. **Proposition 1**

Proof. For any bounded function g , Assumptions 7-8 imply

$$\begin{aligned} \mathbb{E}(g(A)|A_C, \mathbf{X}, U) &= \int g(a) dF_{A|A_C, \mathbf{X}, U}(a) \\ &= \int g(a_{uc} + A_C) dF_{A|A_C, \mathbf{X}, U}(a_{uc}) \\ &= \int g(a_{uc} + A_C) dF_{A|A_C, \mathbf{X}}(a_{uc}) \\ &= \int g(a) dF_{A|A_C, \mathbf{X}}(a) \\ &= \mathbb{E}(g(A)|A_C, \mathbf{X}). \end{aligned}$$

Therefore, for any bounded function f , we have

$$\begin{aligned} \mathbb{E}(g(A)f(U)|A_C, \mathbf{X}) &= \mathbb{E}(f(U)\mathbb{E}(g(A)|A_C, \mathbf{X}, U)|A_C, \mathbf{X}) \\ &= \mathbb{E}(f(U)\mathbb{E}(g(A)|A_C, \mathbf{X})|A_C, \mathbf{X}) \\ &= \mathbb{E}(f(U)|A_C, \mathbf{X})\mathbb{E}(g(A)|A_C, \mathbf{X}). \end{aligned}$$

□

Proposition 2

Proof. Combining Assumption 6 with Proposition 1, the result follows. □

Proposition 3

Proof. By Assumption 5 (consistency) and Proposition 2 (conditional ignorability),

$$\begin{aligned} \mathbb{E}(Y(a)) &= \mathbb{E}(\mathbb{E}(Y(a)|\mathbf{X}, A_C)) \\ &= \mathbb{E}(\mathbb{E}(Y(a)|A, \mathbf{X}, A_C)) \\ &= \mathbb{E}(\mathbb{E}(Y|A = a, \mathbf{X}, A_C)) \\ &= \int \mathbb{E}(Y|A = a, \mathbf{X}, A_C) dF_{A_C, \mathbf{X}}(a_c, x) \end{aligned}$$

for all a where positivity is satisfied, i.e. $\forall a \in \{a' : \text{supp}(A_C, \mathbf{X}) = \text{supp}(A_C, \mathbf{X}|A = a')\}$. Other identifying functionals are also possible. □

S9 Doubly Robust Estimation of the Exposure-Response Curve

Proposition 3 presents one possible identifying functional of the exposure-response curve. However, to protect against model misspecification, we instead use a doubly robust mapping $\xi((X, A_C, A, Y); \pi, \mu)$ whose conditional expectation under exposure equals the causal estimand, as long as the conditional exposure density $\pi(a|x, a_c) = f_{A|X, A_C}(a|X = x, A_C = a_c)$ or outcome mean model $\mu(x, a_c, a) = \mathbb{E}(Y|X = x, A_C = a_c, A = a)$ are correctly specified, following (Kennedy et al., 2017). In particular, defining

$$\xi((X, A_C, A, Y); \pi, \mu) = \frac{Y - \mu(X, A_C, A)}{\pi(A|X, A_C)} \int \pi(A|x, a_c) dF_{X, A_C}(x, a_c) + \int \mu(x, a_c, A) dF_{X, A_C}(x, a_c)$$

we have

$$\mathbb{E}(\xi((X, A_C, A, Y); \bar{\pi}, \bar{\mu})|A = a) = \mathbb{E}(Y(a))$$

if either $\bar{\pi} = \pi$ or $\bar{\mu} = \mu$. This suggests estimating π and μ using off-the-shelf non-parametric regression or machine learning methods and then regressing the pseudo outcome

$$\hat{\xi}((X, A_C, A, Y); \hat{\pi}, \hat{\mu}) = \frac{Y - \hat{\mu}(X, A_C, A)}{\hat{\pi}(A|X, A_C)} \frac{1}{n} \sum_{i=1}^n \hat{\pi}(A|X_i, A_{C_i}) + \frac{1}{n} \sum_{i=1}^n \hat{\mu}(X_i, A_{C_i}, A)$$

on exposure A . The package `npcausal` implements a local linear kernel estimator for the latter regression. Consistency and asymptotic normality of the estimator is proven under additional, reasonably weak assumptions. We made minor modifications to the `ctseff` code in the `npcausal` package to improve functionality. These changes can be found here: <https://github.com/ehkennedy/npcausal/issues/6>.

S10 Additional Simulation Figures

Figure S4 plots one observation of (A, A_{UC}, A_C) for each of the three confounding mechanisms. Table S6 plots the mean and (2.5%, 97.5%) percentile range of the estimated ERCs across the 100 simulations for each of the six confounding scenarios.

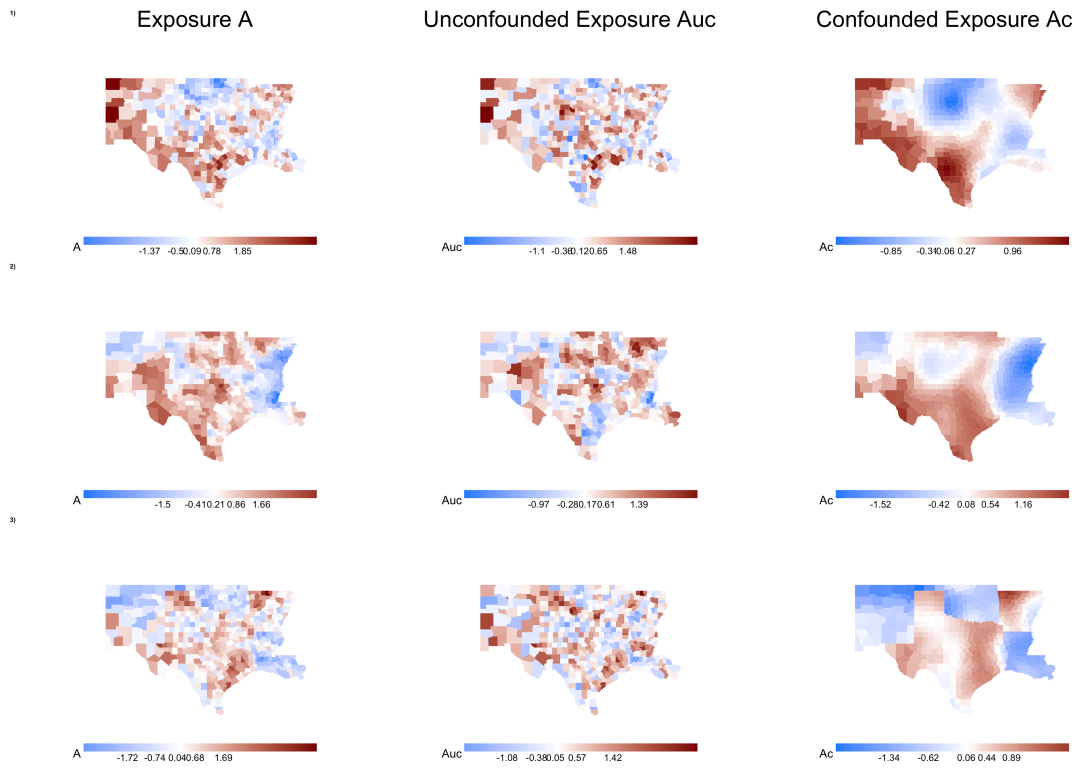


Figure S4: One observation of (A, A_{UC}, A_C) for each of the three confounding mechanisms. Top: first confounding mechanism, $\theta_{AUC} = 0.05$. Middle: second confounding mechanism, $\theta_{AUC} = 0.1$. Bottom: third confounding mechanism, Gaussian process generated within states with $\theta_{AUC} = 0.05$.

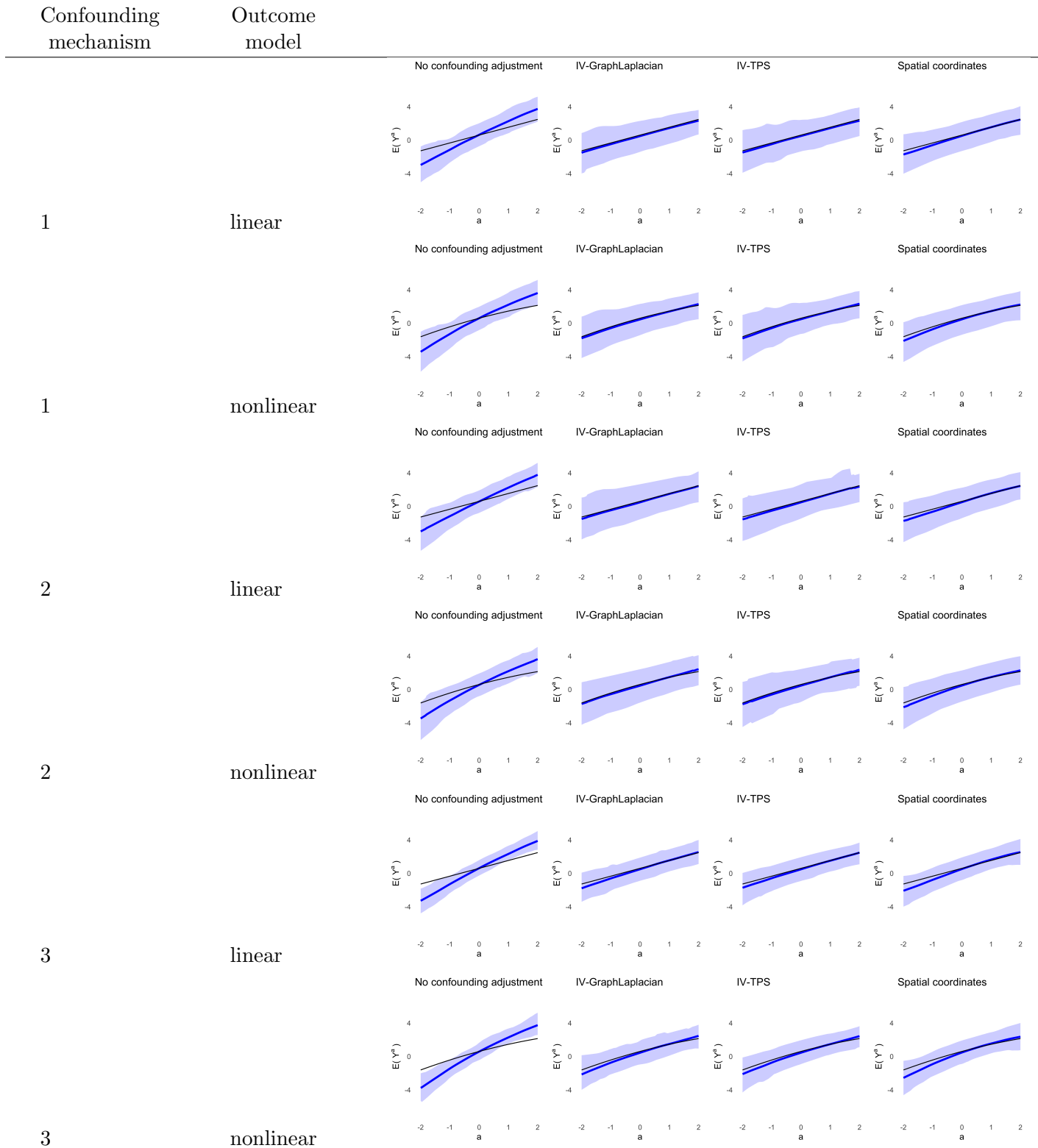


Table S6: Plots of the estimated ERCs. The true ERC is in black. The solid, dark blue line plots the average of the estimated ERCs across the 100 simulations. The light blue band spans the (0.025, 0.975) quantile range of estimated ERCs.